Failure Behavior of Titanium/CFRP Hybrid Composites Under Tensile Loading

[ID] Aysun GÜVEN ÇITIR[a,*], [ID] Serkan TOROS[b,c], [ID] Fahrettin ÖZTÜRK[c,d]

[a] *Department of Mechanical Engineering, Faculty of Engineering, Ankara Yıldırım Beyazıt University, Ankara, TÜRKİYE*
[b] *Department of Mechanical Engineering, Faculty of Engineering, Nigde Omer Halisdemir University, Nigde, TÜRKİYE*
[c] *Turkish Aerospace Industries, Inc., Ankara, TÜRKİYE*
[d] *Faculty of Mechanical Engineering, Istanbul Technical University, Istanbul, TÜRKİYE*
* *Corresponding author: aysunguvencitir@aybu.edu.tr*
DOI: 10.29130/dubited.1472422

ABSTRACT

Carbon fiber reinforced polymer (CFRP) composites have found widespread use in various lightweight engineering applications, owing to their high stiffness and strength at low density. Nevertheless, they exhibit certain weaknesses, such as low bearing strength, leading to reduced impact resistance in CFRP components. In addressing this challenge, metal/CFRP composites have emerged as an alternative, leveraging the ductility of metals along with the high specific strength of the CFRP composites. In this study, tensile tests were conducted on the CFRP composite plates with 0°, 90°, and ±45° stacking sequences, and the corresponding load-displacement curves were obtained. The numerical simulation of tensile tests was conducted by the LS-DYNA software, and the numerical model was verified with the experimental results. Furthermore, numerical simulations were conducted to examine the influence of various metal types on the failure behavior of metal alloy/CFRP hybrid composite plates with different thicknesses under tensile loading. The results indicate that both the thickness of the hybrid CFRP composites and the type of metal have a substantial impact on the performance of metal-hybrid components. Additionally, a comparison between the tensile test results and numerical simulation results reveals a good agreement.

Keywords: Carbon fiber reinforced polymer, CFRP, Failure behavior, Titanium, Hybrid composite plates

Titanyum/CFRP Hibrit Kompozitlerin Çekme Yüklemesi Altındaki Kırılma Davranışı

ÖZ

Karbon fiber takviyeli polimer (CFRP) kompozitler, düşük yoğunlukta yüksek rijitlik ve mukavemetleri nedeniyle çeşitli hafif mühendislik uygulamalarında geniş bir kullanım alanı bulmuştur. Bununla birlikte, CFRP yapıları düşük taşıma mukavemeti gibi belirli zayıflıklar gösterirler, bu durum da CFRP yapılarındaki darbe direncinin azalmasına neden olur. Bu sorunu çözmek için metallerin şekillenebilirliğini ve CFRP kompozitlerin yüksek özgül mukavemeti birlikte kullanılarak metal/CFRP kompozitler bir alternatif olarak ortaya çıkmıştır. Bu çalışmada çekme testleri 0°, 90° ve ±45° istifleme dizilimi ile CFRP kompozit levhalar üzerinde gerçekleştirilmiş ve ilgili yük-şekil değişimi eğrileri elde edilmiştir. Çekme testlerinin sayısal çözümlenmesi, LS-DYNA simülasyon programı kullanılarak gerçekleştirilmiş ve sayısal model deneysel sonuçlarla doğrulanmıştır. Ayrıca, farklı

kalınlıklardaki metal alaşımı/CFRP hibrit kompozit levhaların çekme yüklemesi altındaki kırılma davranışı üzerinde çeşitli metal tiplerinin etkisinin incelenmesi için nümerik simülasyonlar yapılmıştır. Sonuçlar hem hibrit CFRP kompozitlerinin kalınlığının hem de metal tipinin metal-hibrit kompozitlerin performansı üzerinde önemli bir etkisi olduğunu göstermektedir. Ek olarak, çekme testi sonuçları ile sayısal simülasyon sonuçları arasında karşılaştırma yapılmış iyi bir uyum olduğu görülmüştür.

Anahtar Kelimeler: Karbon fiber takviyeli polimer, CFRP, Kırılma davranışı, Titanyum, Hibrit kompozit plakalar

I. INTRODUCTION

In recent decades, fiber reinforced polymer composites (FRPCs) have gained extensive utilization owing to their exceptional mechanical characteristics, including superior strength, stiffness, fatigue resistance, low weight, and manufacturing convenience. However, they have some drawbacks, including low impact and residual strength, susceptibility to moisture, and brittle behavior. To overcome most of these disadvantages, hybrid composite laminates have been introduced to several industries such as aerospace, automotive, defense, and infrastructure [1-3] in various configurations. Fiber metal laminates (FMLs) are hybrid structures based on combining composite laminates and thin metal alloys. Thus, FMLs combines the fatigue and fracture properties of composite laminates with the durability and toughness advantages of metal alloys such as titanium, aluminum, magnesium, and steel [4]. The most commonly used aluminum-based FMLs can be categorized as aramid fiber reinforced aluminum laminate (ARALL), carbon fiber reinforced aluminum laminate (CARALL), and glass fiber reinforced aluminum laminate (GLARE), while titanium-based FMLs are defined as hybrid titanium composite laminates (HTCL).

The mechanical properties of the ARALL, the CARALL, the GLARE, and the HTCL composites have been examined by many researchers [5-9]. Recent studies have demonstrated that various factors influence the mechanical properties of hybrid composite laminates including fiber type, stacking sequence, the adhesion of fiber/metal interlayer and the type of metal/fibers [10-13]. Hynes et al. [14] experimentally and numerically compared the mechanical properties of the CFRP to the FMLs, which consist of Al6061 (0.5 mm thickness) and the CFRP combined in two different stacking sequences. The stacking sequence of laminates, which start and end with Al6061 and the CFRP respectively, was labeled as Type-I (ACACA) and Type-II (CACAC), while a laminate consisting solely of the CFRP was defined as Type-III. The results revealed that the stacking sequence significantly influences mechanical properties including tensile strength, impact resistance, and flexural strength. For example, Type-I and Type-II FMLs demonstrated 24.40% and 6.41% higher tensile strength, 79.56% and 55.93% higher impact energy, and 51.61% and 37.5% greater ultimate breaking load compared to the CFRP, respectively. Sun et al. [15] investigated the effect of strain rate on the mechanical properties such as tensile strength of titanium based and aluminum based FMLs. Ti6Al4V and AL2024 were preferred as metal alloys, and both combined with the CFRP. They concluded that strain rate has negligible effect on the mechanical properties of these FMLs. Furthermore, the HTCLs were showed higher specific strength than the CARALLs. Yao et al. [16] examined the tensile strength and damage mechanisms of the FMLs at different temperatures also regarding the effect of the orientation of the layers by experimentally, numerically, and theoretically. T700/3234 CFRP and 2024-T3 aluminum, a thickness of 0.5 mm, were tested at different temperatures with different layer orientation. It was concluded that the orientation of the layers in the FMLs significantly influences their final fracture sequence and failure mechanism. In the FMLs with layers oriented at 0°/90° and 45°/−45°, the final damage mode is primarily driven by the fibers, indicating a tension-dominated failure mechanism, and the aluminum layers, indicating a tension-shear dominated failure mechanism, respectively. It implies that the arrangement of layers not only affects the overall mechanical behavior of the laminate but also determines how the laminate responds to stress and ultimately fails. Additionally, the FMLs primarily exhibit fiber fracture and matrix cracking at low temperatures while there is more delamination between metal alloy and composite layers at high temperatures which causes sudden decrease in ultimate tensile load. Sharma and Velmurugan [17] conducted a study on the tensile characterization of the FMLs composed of

Ti6Al4V sheets and of glass fiber reinforced polymer (GFRP) composite layers. They examined the FMLs with varying thicknesses of Ti6Al4V sheets, where metal layers were dispersed throughout the thickness while maintaining a constant total thickness for the metal layer. Additionally, they investigated different stacking sequences of the GFRP under tension. The FMLs with grouped composite layers exhibited higher strength compared to the FMLs with discrete metal layers. Additionally, the FMLs with dissimilar fiber orientations separated by a metal layer demonstrated increased tolerance to damage with only minor reductions in strength.

In this study, it was aimed to investigate mechanical properties of metal/CFRP hybrid composite laminates under tensile loading. The tensile behavior of the CFRP composite laminates were tested experimentally according to ASTM D3039 for 0° and 90° and ASTM D3518 for ±45° stacking sequences. Additionally, hybrid composite laminates with varying thicknesses of metal layers (0.3 mm and 0.6 mm) and different types of metal alloys (Ti6Al4V, Al7075-T6, Al6061-T6, and Al2024-T3) were examined through finite element analysis (FEA) utilizing the LS-DYNA software.

II. MATERIALS AND METHOD

A. MATERIALS

UD (unidirectional) carbon fiber reinforced LM-PAEK (Cetex® TC1225) with a 34% resin content by weight was supplied by Toray Industries, Inc. The physical and mechanical properties of the UD/CFRP composites supplied from technical data sheets provided by the manufacturer are given in Table 1.

Table 1. Material properties of considered CFRP composite.

| Properties	LM-PAEK
Density (g/cm^3)	1.3
Modulus (GPa)	E11=135; E22=E33=10; G12=G13= G23= 4.3
Poisson's ratio	υ12= υ13= υ23=0.33
Tensile strength 0° (MPa)	XT=2410
Tensile strength 90° (MPa)	YT=86
Shear strength (MPa)	SC=152

B. FABRICATION OF SPECIMENS

The UD/CFRP composite specimens were produced according to ASTM D3039 for 0° and 90° stacking sequences and ASTM D3518 for ±45° stacking sequences, each with different lay-ups: 90° and ±45° stacking sequences with 16 plies and 0° with 8 plies. The thickness of each layer is 0.140 mm. The manufacturing process CF/LM-PAEK prepregs were shown in Figure 1.

Cutting samples by CNC   Spot welding   Autoclave process   Tensile test samples
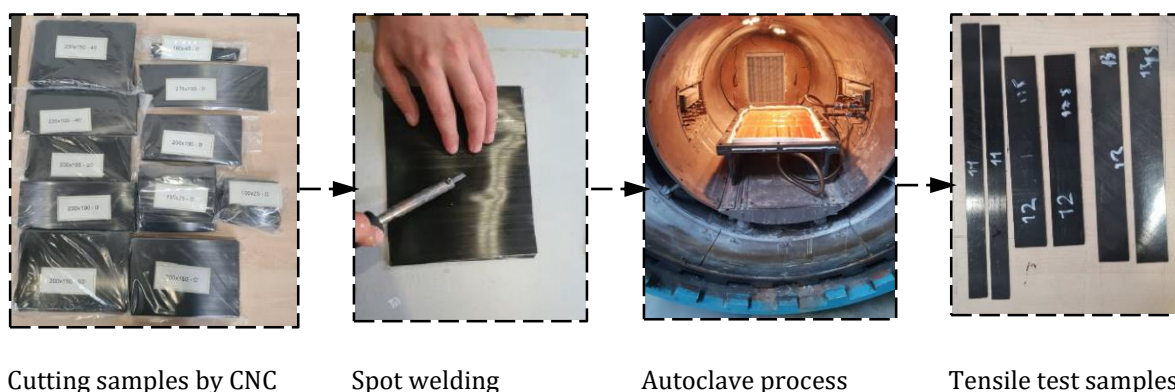
Figure 1. Manufacturing process of CFRP composites.

Initially, the prepregs were cut using CNC and arranged in the desired directions. A spot-welding process was then performed at two edges and one in the center of the plates to prevent any slippage or displacement. Subsequently, the prepregs were heated in an autoclave at a specified temperature and pressure. Two different autoclave cycles were used for LM-PAEK and PEKK composite consolidation with Ti6Al4V. The curing cycle of LM/PAEK was carried out at a heating rate of 3 °C/min up to 260°C for first heating cycle and with a heating rate of 3 °C/min up to 370°C for second heating cycle. Then return to room temperature at a heating rate of 3 °C/min. The curing cycle of PEKK was performed at a heating rate of 11 °C/min up to 400°C and was held at 400°C for 3 h, then return to room temperature at a heating rate of 3 °C/min. The vacuum of 0.08 MPa was used for both LM/PAEK and PEKK autoclave cycles. Finally, the prepared prepreg layers were precision-cut to the required dimensions for tensile testing, employing a water jet cutting technique.
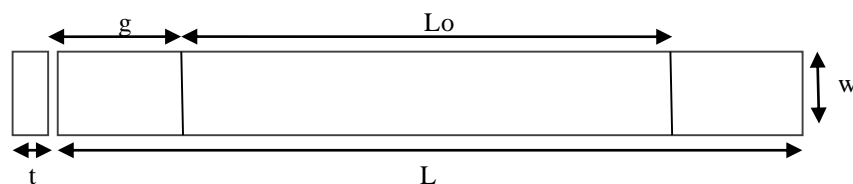
Figure 2. The overall dimensions and layout of the UD/CFRP tensile test specimen.

The general specimen layout of the UD/CFRP composite laminate shown in Figure 2. The length, width and thickness values of the tensile test specimens varied depending on their respective ASTM standards. The dimensions of 0° direction test coupon, which has 8 plies with the layup configuration of $[0°]_8$, and the dimensions of 90° direction test coupon, which has 16 plies with the layup configuration of $[90°]_{16}$, were chosen as suggested in ASTM D3039 standard detailed in Table 2. Additionally, according to ASTM D3518 standard, the value of n for unidirectional composites is recommended to be within the range of $4 \leq n \leq 6$. Therefore, the value of n was selected as four, resulting in the production of (±45°) test coupons with 16 plies.

Table 2. Details of LM-PAEK tensile specimens.

Material	Layup	Length, L (mm)	Width, w (mm)	Thickness, t (mm)	Gage length, Lo (mm)	Grip length, g (mm)	ASTM standard
LM_PAEK	$[0°]_8$	250	15	1	130	60	ASTM D3039
	$[+45/-45°]_{4s}$	200	25	2	50	50	ASTM D3518
	$[90°]_{16}$	175	25	2	40	40	ASTM D3039

C. TESTING OF COMPOSITE SPECIMENS

.

The tensile properties of unidirectional the CFRP composite specimens were tested at room temperature (RT) using a Shimadzu AGS-X 100kN universal testing machine using a constant crosshead speed of 2 mm/min according to ASTM D3039 for 0° and 90°, and ASTM D3518 for ±45° stacking sequences. Five repeated tensile tests were conducted to minimize any experimental inaccuracies. Figure 3 shows the UD/CFRP tensile test specimen loaded in the universal testing machine.
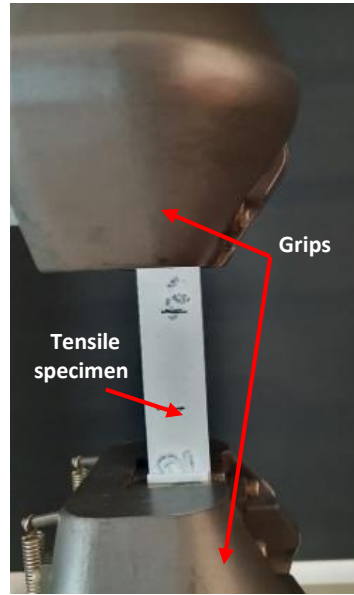
Figure 3. *Specimen loaded in a Shimadzu AGS-X 100kN universal testing machine.*

III. NUMERICAL SIMULATIONS

Tensile test simulations on the CFRP composite laminates and the hybrid composite laminates were performed by the quasi-static implicit solver in the LS-DYNA software using the geometry as defined in the tensile experiment tests. Figure 4 illustrates the side view of the hybrid laminate composites with varying thicknesses, represented by shell elements. To show the contrast in thickness between the metal layers, which are 0.3 mm and 0.6 mm in the simulations, the "shell thickness effect" option was applied to all layers.

Figure 4. *The side view of a FEM model of the hybrid composite laminates tensile test specimens.*

Table 3 shows the details of hybrid composite laminates used in the numerical simulations. Additionally, $[0°]_8$, $[\pm 45°]_8$ and $[90°]_{16}$ stacking sequences of the UD/CFRP laminates were defined as LM-PAEK/A, LM-PAEK/B, and LM-PAEK/C, respectively.

Table 3. *Details of the hybrid laminates.*

Notation	Layup sequence	Metal alloy	Metal thickness *(mm)*	Total thickness *(mm)*
Ti_0.3/A		Ti6Al4V	0.3	1.42
Ti_0.6/A			0.6	1.72
Al1_0.3/A		Al7075-T6	0.3	1.42
Al1_0.6/A			0.6	1.72
Al2_0.3/A	$[0°]_4$ /Metal alloy/$[0°]_4$	Al2024-T3	0.3	1.42
Al2_0.6/A			0.6	1.72
Al3_0.3/A		Al6061-T6	0.3	1.42
Al3_0.6/A			0.6	1.72

Table 3 (cont). Details of the hybrid laminates.

Ti_0.3/B	[±45°]₄/Metal alloy/[±45°]₄	Ti6Al4V	0.3	1.42
Ti_0.6/B			0.6	1.72
Al1_0.3/B		Al7075-T6	0.3	1.42
Al1_0.6/B			0.6	1.72
Al2_0.3/B		Al2024-T3	0.3	1.42
Al2_0.6/B			0.6	1.72
Al3_0.3/B		Al6061-T6	0.3	1.42
Al3_0.6/B			0.6	1.72
Ti_0.3/C	[90°]₈/Metal alloy/[90°]₈	Ti6Al4V	0.3	2.54
Ti_0.6/C			0.6	2.84
Al1_0.3/C		Al7075-T6	0.3	2.54
Al1_0.6/C			0.6	2.84
Al2_0.3/C		Al2024-T3	0.3	2.54
Al2_0.6/C			0.6	2.84
Al3_0.3/C		Al6061-T6	0.3	2.54
Al3_0.6/C			0.6	2.84

The tensile behavior of the UD/CFRP composite materials was modelled using the MAT54 (*MAT_ENHANCED_COMPOSITE_DAMAGE) material card, specifically designed to handle orthotropic materials like the UD tape composite laminates and based on the Chang-Chang failure criterion. All plies of the CFRP composite were assembled with *PART_COMPOSITE_LONG card with different stacking sequences. *MAT_098 (SIMPLIFIED_JOHNSON_COOK) keyword was used to define an isotropic elasto-plastic material including Ti6Al4V, Al7075-T6, Al2024-T3, and Al6061-T6 metal alloys. The general material properties and the Johnson-Cook model parameters of Ti6Al4V, Al7075-T6, Al6061-T6, and Al2024-T3 metal alloys used in the simulations given in Table 4 and 5, respectively.

Table 4. General material properties of Ti6Al4V, Al7075-T6, Al6061-T6, and Al2024-T3 [18,19].

| Properties	Ti6Al4V	Al7075-T6	Al6061-T6	Al2024-T3
Young modulus, E (GPa)	109.8	71.7	68.9	70
Poisson's ratio, υ	0.31	0.33	0.33	0.3
Density, ρ (kg/m³)	4428	2810	2700	2700

Table 5. The Johnson-Cook model parameters of Ti6Al4V, Al7075-T6, Al6061-T6, and Al2024-T3 [18,19].

| Materials	A (MPa)	B (MPa)	n	C	m
Ti6Al4V	1098	1092	0.93	0.014	1.1
Al7075-T6	546	678	0.71	0.024	1.56
Al6061-T6	289	203.4	0.35	0.011	1.34
Al2024-T3	352	440	0.42	0.0083	1.7

The metal alloy layers and the CFRP composite layers were bonded together using the *CONTACT_TIED_SURFACE_TO_SURFACE contact card in the LS-DYNA software. Specifically, no contact definition was applied to the CFRP composite layers, as each layer was defined in the simulation using the PART_COMPOSITE_LONG card.

The boundary conditions of the tensile samples in the LS-DYNA software were adjusted to correspond with those of the uniaxial tensile experiment. During the uniaxial tensile test, one end tab of the samples was clamped with six degrees of freedom (DOF) fixed while the other end tab underwent a displacement. Figure 5 shows the boundary conditions of the numerical model used in the simulations.
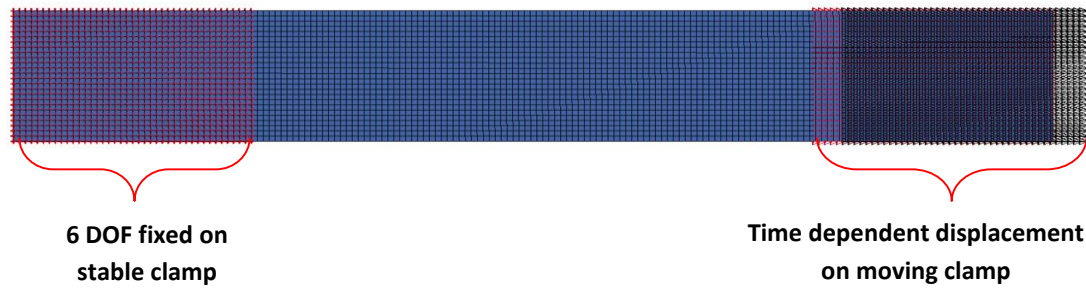
Figure 5. The boundary conditions of the numerical model.

In numerical modelling, the mesh sizes have significant effect on the accuracy of the model. Therefore, it is important to determine the appropriate mesh size of the numerical model to minimize computational time and resources. For this reason, seven different element sizes for the uniaxial tensile test coupon were simulated with 0.125, 0.25, 0.5, 1, 2, 4, 8 mm first order quad elements as shown in Figure 6.

| 0.125 mm | 0.25 mm | 0.5 mm | 1 mm | 2 mm | 4 mm | 8 mm |
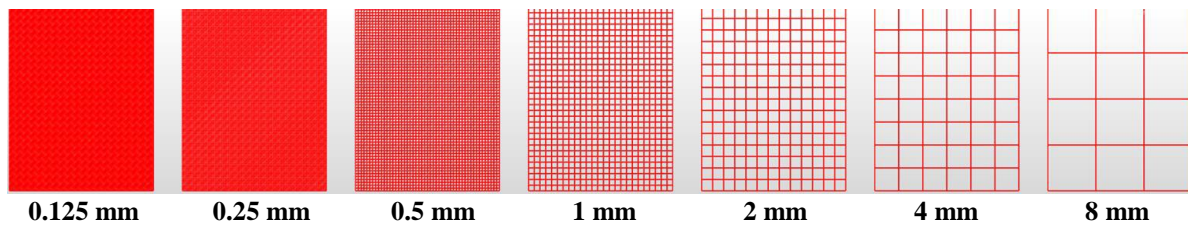
Figure 6. Element sizes of the numerical model for mesh sensitivity analysis.
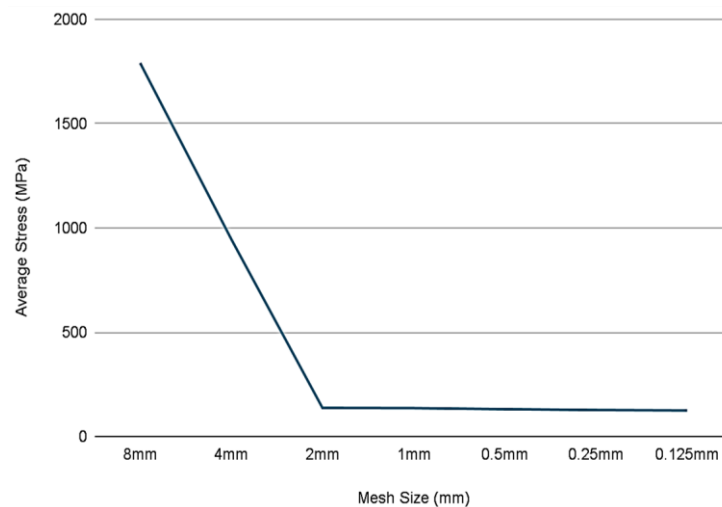
*Figure 7. Average stress vs. mesh size graph.*

Figure 7 shows the average stress response for different mesh sizes of the tensile test coupons. The graph was created by selecting the peak values of the time-dependent the von-Mises stress average of all elements on the sample. As increasing the mesh size, the computational time increase. However, as the element size decreased, especially from 8 mm to 2 mm, the average stress line decreased dramatically, and the accuracy of the model was increased.

Especially, after the 2 mm mesh size, the results were slightly changed by the more refined mesh size. The 1 mm element size (number of elements=5000), which has the most optimum analysis accuracy percentage and solution time ratio, was chosen to be used in analysis models, despite achieving fast and fairly accurate analysis solutions with 2 mm element size (number of elements=1300).

IV. RESULTS AND DISCUSSION

A. MECHANICAL TESTING

Three different types of stacking sequences were tested under tensile loading to investigate their fracture behavior and strength. The uniaxial tensile test specimens before the tests shown in Figure 8 (a). The failure mode of 90° UD/CFRP laminates was observed along to the transverse direction of loading while the failure mode of the ±45° specimens was observed along the diagonal direction of loading due to the rotation of the fibers during the tensile test as shown in Figure 8 (b).

(a)   **(b)**
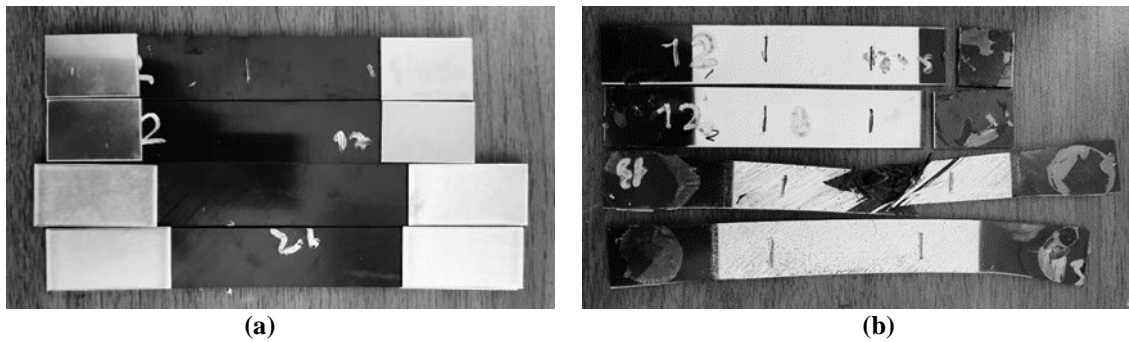
Figure 8. The CFRP tensile test specimens with 90° and ±45° stacking sequences (a) before and (b) after tensile tests.
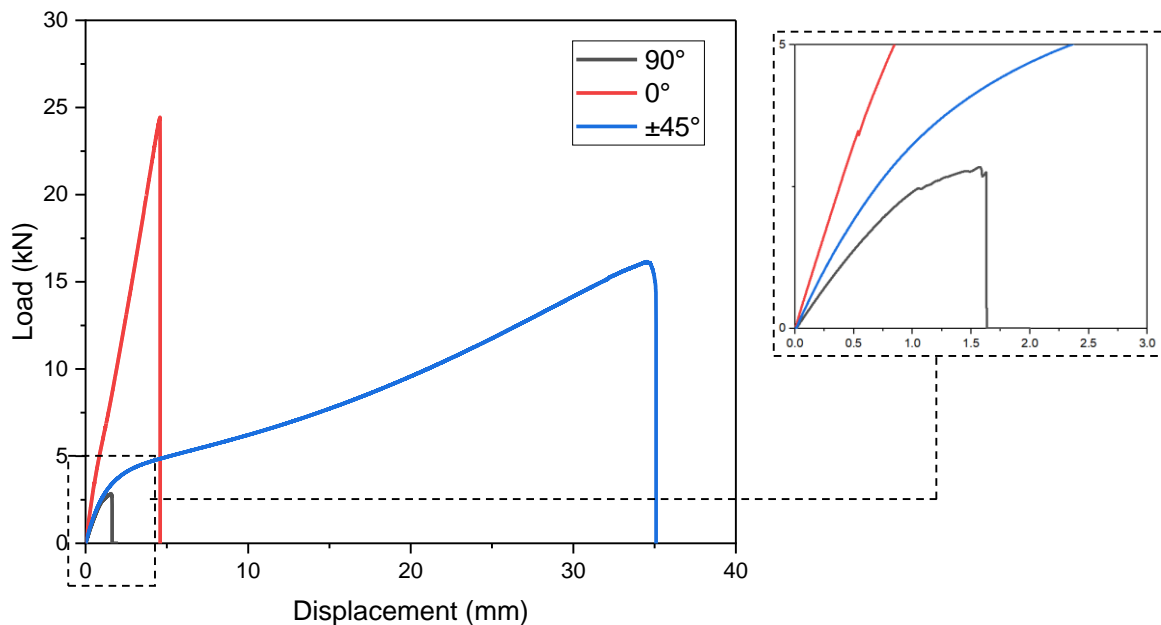
Figure 9. Load-displacement tensile test results for the CFRP composites.

The load-displacement curves derived from the experimental results for three different stacking sequences, depicted in Figure 9, also include a zoomed-in view of the low load region. The maximum loads observed for the CFRP with a stacking sequences of 0°, 90°, and ±45° were determined to be 24.44 kN, 2.82 kN, and 16.16 kN, respectively. Therefore, the highest maximum load was recorded for the 0° stacking sequence, whereas the lowest was observed for the 90° stacking sequence [20,21]. It can be concluded that the 0° orientation carries the highest load due to the longitudinal direction while the 90° orientation carries the lowest load due to the perpendicular direction [22]. Regarding displacement, the maximum displacement measured was 35.1 mm for the ±45° stacking sequence, whereas the lowest displacement was 1.63 mm for the 90° stacking sequence. Additionally, the tensile strengths of the

UD/CFRP composites in the 0°, 90°, and ±45° directions were nearly 1630 MPa, 57 MPa, and 162 MPa, respectively.

B. NUMERICAL MODELLING

Initially, the load-displacement curves of the FE model results were compared to the experimental results for the UD/CFRP composite laminates to validate the material and geometric models used in the FE model. Figure 10 (a), (b), and (c) illustrate the load-displacement curves for the numerical and experimental results of the CFRP laminates with $[0°]_8$, $[\pm45°]_8$, and $[90°]_{16}$ stacking sequences, respectively. The 0° specimen for both experimental and numerical results displayed linear increase before fracture on the load-displacement curves. The 90° specimen initially responded with a linear increase, then the curve oscillated slightly as it approached the fracture point. The ±45° specimen for experimental and numerical results showed similar slope changes until failure occurred. The average error of the maximum loads between the numerical and experimental results for $[0°]_8$, $[\pm45°]_8$ and $[90°]_{16}$ stacking sequences of the CFRP composite laminates shown in Table 6. It was found that a good agreement was achieved between the numerical and the experimental results. Therefore, the FE model used for further investigations of the hybrid composite laminates.

Table 6. *The average error of the experimental and the numerical results.*

| Layup	Maximum load (kN)		Error (%)
	Experimental	Numerical	
$[0°]_8$	24.44	27.8	13.74
$[+45/-45°]_8$	16.16	17.1	5.81
$[90°]_{16}$	2.82	2.42	14.18
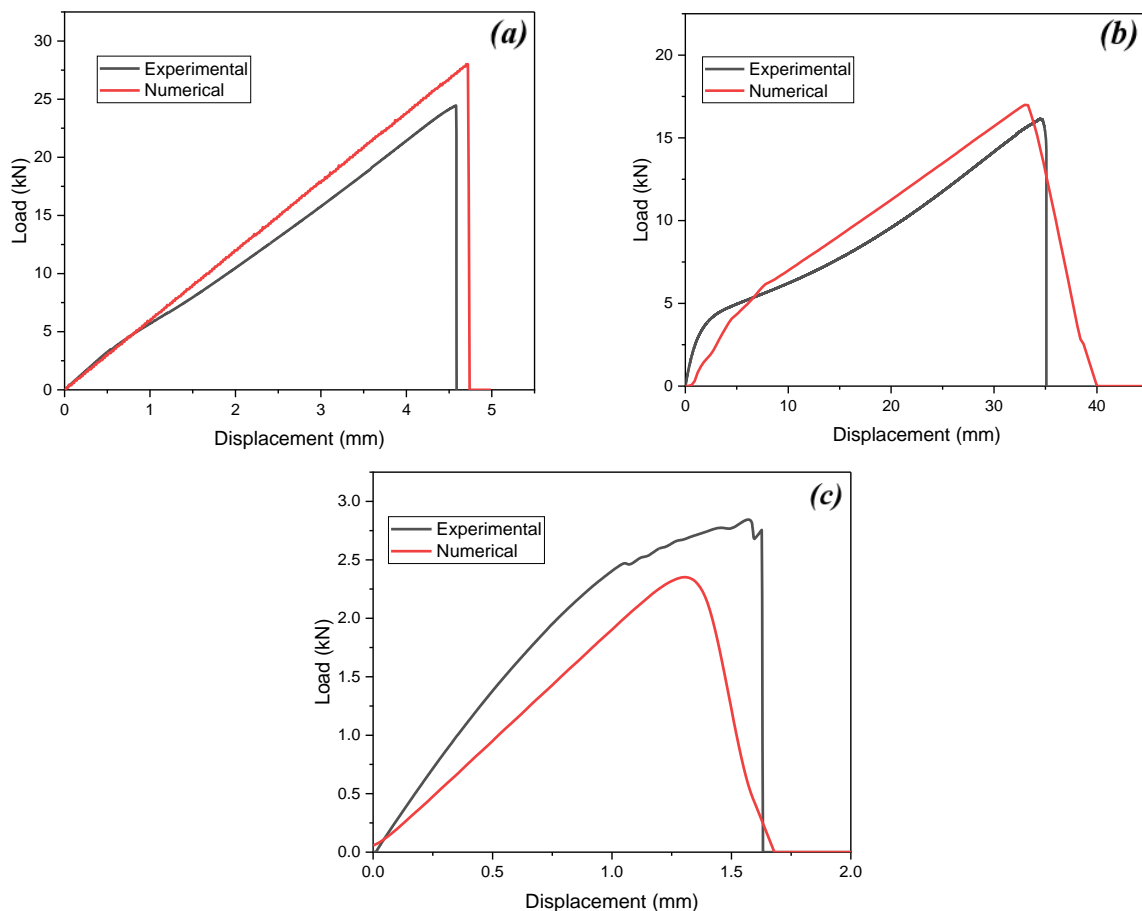
Figure 10. *Load-displacement curves of the FE model and experiment of the CFRP composite laminate for (a) $[0°]_8$, (b) $[\pm45°]_8$, (c) $[90°]_{16}$.*

2323

Figure 11, 12, and 13 shows the fracture behavior of the CFRP composite laminates at selected times under uniaxial tensile loading for $[0°]_8$, $[\pm45°]_8$, and $[90°]_{16}$ stacking sequences, respectively. The effective stress of the CFRP composite laminate, oriented in 0° direction, increases with the increasing displacement between the two clamps over time, as illustrated both in Figure 11 (a) and 11 (b). The failure has been observed perpendicular to the orientation direction when the specimen has reached its ultimate tensile strength, in Figure 11 (c).
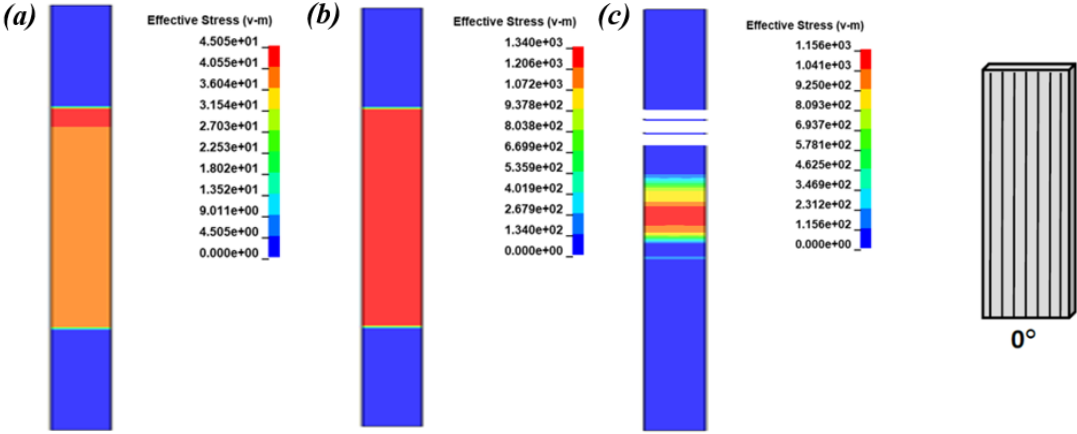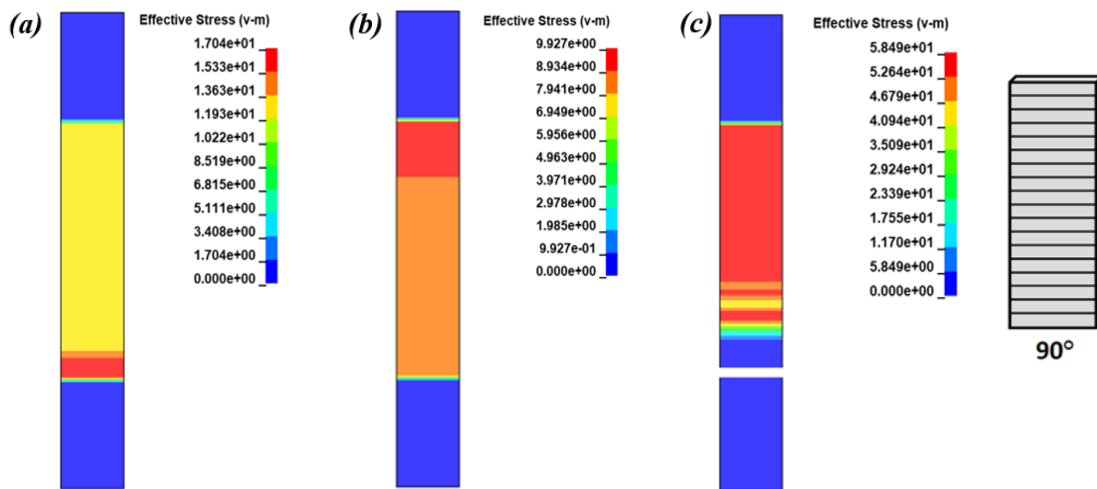

Figure 11. *Fracture behavior of the UD/CFRP composite laminate with $[0°]_8$ stacking at (a) 0.002s (b) 0.035s, and (c) 0.048s.*

Similar to the 0° specimen, the effective stress values of the CFRP composite laminate in the ±45° direction have increased as displacement increases as seen in Figure 12. However, when the specimen reached ultimate tensile strength, the failure was observed at ±45° orientation in different failure pattern than both 0° and 90° specimens as in the experiment. In Figure 13, the 90° specimen had a similar failure pattern to the 0° specimen. The highest stress was observed in the 0° specimen and the lowest was in the 90° specimen, as found in the experiment. Briefly, the results also demonstrated that the failure modes of three different stacking sequences were similar to those observed in the experimental tests.
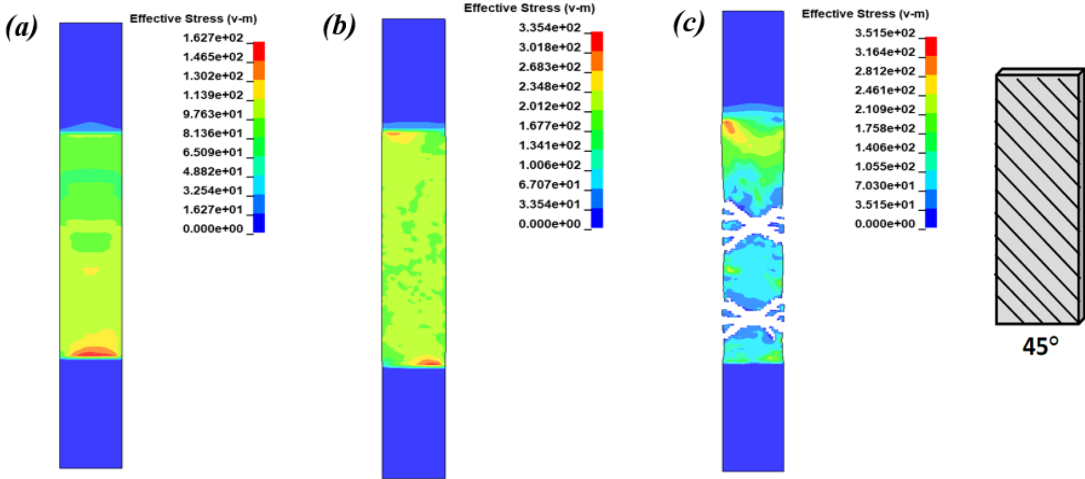

Figure 12. *Fracture behavior of the UD/CFRP composite laminate with $[\pm45°]_8$ stacking at (a) 0.002s (b) 0.005s, and (c) 0.012s.*

*Figure 13. Fracture behavior of the UD/CFRP composite laminate with [90°]₁₆ stacking at (a) 0.002s (b) 0.004s, and (c) 0.016s.*

The comparison of the load-displacement curves of the hybrid composite laminates for the 0° stacking sequences shown in Figure 14. Ti_0.6/A demonstrated the highest strength with the highest maximum load of 38.1 kN while PAEK/A showed the lowest strength with the maximum load of 28 kN. Ti6Al4V sheets improved the strength of the hybrid composite laminates in the 0° orientation to a greater extent compared to the improvement provided by aluminum alloy sheets especially with the thickness of 0.6 mm metal alloy layer. The maximum load value for Ti_0.6/A was 38.1 kN and for Al1_0.6/A, Al2_0.6/A and Al3_0.6/A were 33.27 kN, 31.8 kN and 31.03 kN, respectively. Therefore, the Ti6Al4V sheet, has a thickness of 0.6 mm, improved the maximum load 14.5%, 19.81%, and 22.78% greater than Al7075-T6, Al6061-T6, and Al2024-T3 alloy, respectively. The maximum load value for Ti_0.3/A was 33.1 kN and for Al1_0.3/A, Al2_0.3/A and Al3_0.3/A were 33.27 kN, 29.9 kN and 29.5 kN, respectively. It can be concluded that the FMLs had higher strength values than the CFRP composites [14].
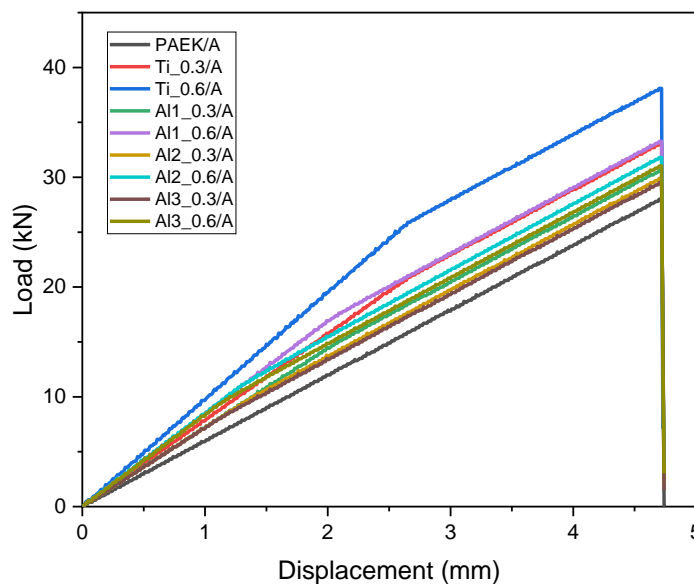
Figure 14. Load-displacement curves of the FE model for the CFRP and the hybrid composite laminates with the 0° stacking sequences.

The comparison of the load-displacement curves of the hybrid composite laminates for the ±45° stacking sequences shown in Figure 15. The highest maximum load value for the hybrid composite laminates in

the ±45° samples was 34.42 kN and it occurred on "Ti_0.6/B" while the lowest value was 16.98 kN of PAEK/B. The maximum load value for Ti_0.6/B was 34.42 kN and for Al1_0.6/B, Al2_0.6/B and Al3_0.6/B were 26.7 kN, 26.8 kN, and 24.25 kN, respectively. The maximum load value for Ti_0.3/B was 24.21 kN and for Al1_0.3/B, Al2_0.3/B and Al3_0.3/B were 20.19 kN, 19.96 kN, and 18.24 kN, respectively.
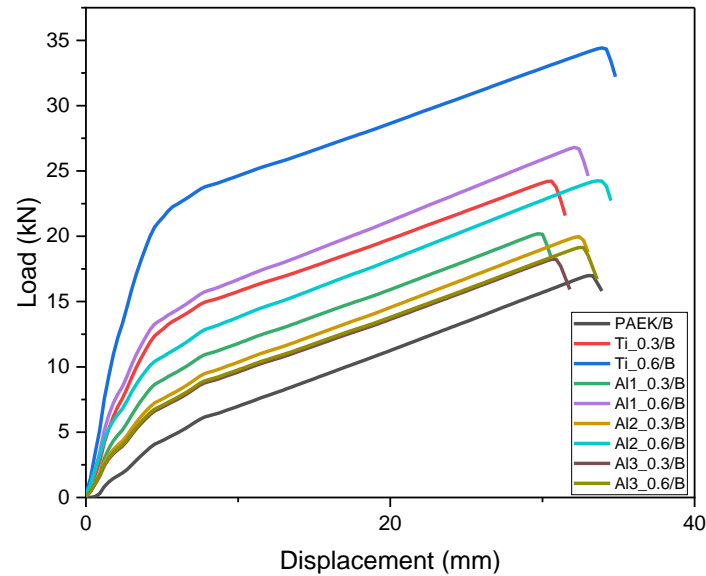
Figure 15. *Load-displacement curves of the FE model for the CFRP and the hybrid composite laminates with the ±45° stacking sequences.*
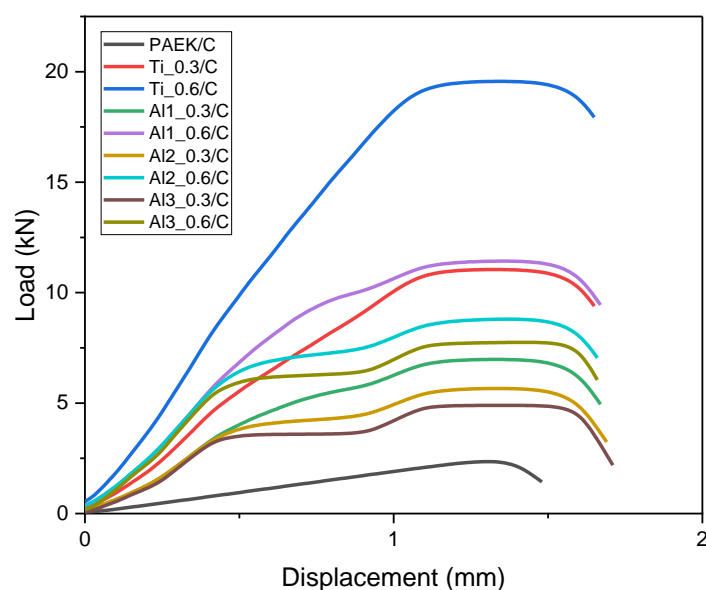
The comparison of the load-displacement curves of the hybrid composite laminates for the 90° stacking sequences shown in Figure 16. The highest maximum load value for the hybrid composite laminates in the 90° samples was 19.56 kN and it occurred on "Ti_0.6/C" while the lowest value was 2.35 kN of PAEK/C. The maximum load value for Ti_0.6/C was 19.56 kN and for Al1_0.6/C, Al2_0.6/C, and Al3_0.6/C were 11.42 kN, 8.8 kN, and 7.75 kN, respectively. The maximum load value for Ti_0.3/C was 11.04 kN and for Al1_0.3/C, Al2_0.3/C, and Al3_0.3/C were 6.97 kN, 5.66 kN, and 4.9 kN, respectively.

Figure 16. *Load-displacement curves of the FE model for the CFRP and the hybrid composite laminates with the 90° stacking sequences.*

In summary, when comparing the effects of the metal alloys with a thickness of 0.6 mm used in the configurations of the hybrid composite laminates, it is obvious that Ti6Al4V substantially improves the tensile strength and has the highest effect on the tensile strength for all three stacking sequences [23]. Furthermore, Al7075-T6 demonstrates peak load values of 33.27 kN, 27.53 kN, and 11.42 kN for the 0°, ±45°, and 90° orientations, respectively. Regarding the maximum load values improvement, the metal alloys can be listed in descending order as follows: Ti6Al4V, Al7075-T6, Al6061-T6, and Al2024-T3 for all three stacking sequences [14-16]. It can be concluded that the types of the metal alloy layers have a significant effect on the strength of the hybrid composite laminates. When comparing the thickness of the metal alloy layers at 0.3 mm and 0.6 mm in terms of the maximum loads, the most significant difference was observed in the Ti6Al4V alloy hybrid composite laminates for all three stacking sequences. The other metal alloys used in the configurations, with thicknesses of both 0.3 mm and 0.6 mm, exhibited slightly different maximum load values. It was found that as the thickness of the metal alloy layer increased, the strength of the hybrid composite laminates significantly increased for Ti6Al4V, while it only showed a slight increase for all aluminum alloys including Al7075-T6, Al6061-T6, and Al2024-T3 [24].

V. CONCLUSIONS

In this research, LM-PAEK specimens were manufactured and tested by the uniaxial tensile testing machine. The mechanical properties of the LM-PAEK were examined by experimentally and numerically. The results of experiments and numerical simulations were compared and verified the numerical model. By using the verified numerical model, the different metal types (Ti6Al4V, Al7075-T6, Al6061-T6, and Al2024-T3) and different metal thickness values (0.3 mm and 0.6 mm) were investigated by the FEM simulations using the LS-DYNA software to determine their effects on the mechanical properties on the hybrid composite laminates. The overall results were drawn as follows:

- In the numerical simulations, the maximum displacements of the hybrid composite laminates were around 4.7 mm and 1.48 mm for the 0° and the 90° UD/CFRP samples, respectively, while it was approximately 40 mm for the ±45° UD/CFRP samples. Additionally, the maximum loads of the samples were highest in the 0° direction, followed by the ±45°, and the 90° directions for these samples.

- The Ti_0.6/A specimen had the highest maximum load, 38.1 kN, among the hybrid laminate composites and the lowest maximum load was 28 kN for the LM-PAEK/A for the 0° samples. The titanium sheet with a thickness of 0.6 mm provided a 36.1% increase in the maximum load compared to the LM-PAEK/A.

- The Ti_0.6/B specimen had the highest maximum load among the hybrid laminate composites with a value reaching 34.42 kN and the lowest maximum load was 16.98 kN for the LM-PAEK/B for the ±45° samples. Ti_0.6/B specimen reached the maximum load almost 2 times that of the UD/CFRP in the ±45° direction.

- The Ti_0.6/C specimen had the highest maximum load among the hybrid laminate composites with a value reaching 19.56 kN and the lowest maximum load was 2.35 kN for the LM-PAEK/C for the 90° samples. Ti_0.6/C specimen reached the maximum load 8.32 times that of the UD/CFRP in the 90° direction.

- Al7075-T6 specimen in the 0° direction had the highest maximum load among Al6061-T6, and Al2024-T3 hybrid laminate composite for both 0.6 mm and 0.3 mm thickness. The tensile strength of Al1_0.6/A was 2218 MPa while Al2_0.6/A and Al3_0.6/A were 2120 MPa and 2068 MPa, respectively.

- Al7075-T6 specimen in the 0° direction had the highest maximum load among Al6061-T6, and Al2024-T3 hybrid laminate composite for both 0.6 mm and 0.3 mm thickness. The tensile strength of Al1_0.6/A was 2218 MPa while Al2_0.6/A and Al3_0.6/A were 2120 MPa and 2068 MPa, respectively.

VI. REFERENCES

[1]　T. Sinmazçelik, E. Avcu, M. Ö. Bora, and O. Çoban, "A review: Fibre metal laminates, background, bonding types and applied test methods," *Materials & Design (1980-2015)*, vol. 32, no. 7, pp. 3671–3685, Mar. 2011.

[2]　A. Vlot and J. W. Gunnink, *Fibre metal laminates:an introduction*, 2001.

[3]　L. B. Vogelesang and A. Vlot, "Development of fibre metal laminates for advanced aerospace structures," *J. Mater. Process. Technol.*, vol. 103, no. 1, pp. 1–5, 2000. L. B. Vogelesang and A. Vlot, "Development of fibre metal laminates for advanced aerospace structures," *Journal of Materials Processing Technology*, vol. 103, no. 1, pp. 1–5, Jun. 2000.

[4]　R. Alderliesten, *Fatigue and Fracture of Fibre Metal Laminates*, 2017.

[5]　C. Bellini, V. Di Cocco, F. Iacoviello, and L. Sorrentino, "Failure energy and strength of Al/CFRP hybrid laminates under flexural load," *Material Design & Processing Communications*, vol. 2, no. 5, Nov. 2019.

[6]　Nassier. A. Nassir *et al.*, "Experimental and numerical characterization of titanium-based fibre metal laminates," *Composite Structures*, vol. 245, p. 112398, Apr. 2020.

[7]　C. Chu, L. Shan, M. S. H. Al-Furjan, Zarei, M. H. Hajmohammad, and R. Kolahchi, "Experimental study for the effect of hole notched in fracture mechanics of GLARE and GFRP composites subjected to quasi-static loading," *Theoretical and Applied Fracture Mechanics*, vol. 122, p. 103624, Oct. 2022.

[8]　S. Yogesh and S. Madhu, "Mechanical properties evaluation of the Al reinforced CFRP fiber metal laminate," *Materials Today Proceedings*, vol. 33, pp. 44–47, Jan. 2020.

[9]　G.-C. Yu, L.-Z. Wu, L. Ma, and J. Xiong, "Low velocity impact of carbon fiber aluminum laminates," *Composite Structures*, vol. 119, pp. 757–766, Jan. 2015.

[10]　M. E. Kazemi *et al.*, "Developing thermoplastic hybrid titanium composite laminates (HTCLS) at room temperature: Low-velocity impact analyses," *Composites Part a Applied Science and Manufacturing*, vol. 149, p. 106552, Jul. 2021.

[11]　M. E. Kazemi, L. Shanmugam, L. Yang, and J. Yang, "A review on the hybrid titanium composite laminates (HTCLs) with focuses on surface treatments, fabrications, and mechanical properties," Compos. Part A Appl. Sci. Manuf., vol. 128, 2020.

[12]　R. C. Santiago, W. J. Cantwell, N. Jones, and M. Alves, "The modelling of impact loading on thermoplastic fibre-metal laminates," *Composite Structures*, vol. 189, pp. 228–238, Feb. 2018.

[13]　E. C. Botelho, R. A. Silva, L. C. Pardini, and M. C. Rezende, "A review on the development and properties of continuous fiber/epoxy/aluminum hybrid composites for aircraft structures," *Materials Research*, vol. 9, no. 3, pp. 247–256, Sep. 2006.

[14]   N. Rajesh *et al.*, "Effect of stacking sequence of fibre metal laminates with carbon fibre reinforced composites on mechanical attributes: Numerical simulations and experimental validation," *Composites Science and Technology*, vol. 221, pp. 109303–109303, Apr. 2022.

[15]   J. Sun, S. Xu, G. Lu, D. Ruan, and Q. Wang, "Mechanical response of fibre metal laminates (FMLs) under low to intermediate strain rate tension," *Composite Structures*, vol. 305, p. 116493, Nov. 2022.

[16]   L. Yao, S. Zhang, X. Cao, Z. Gu, C. Wang, and W. He, "Tensile mechanical behavior and failure mechanisms of fiber metal laminates under various temperature environments," *Composite Structures*, vol. 284, p. 115142, Jan. 2022.

[17]   A. P. Sharma and R. Velmurugan, "Uni-axial tensile response and failure of glass fiber reinforced titanium laminates," *Thin-Walled Structures*, vol. 154, p. 106859, Jun. 2020.

[18]   D. García-González, M. Rodríguez-Millán, A. Vaz-Romero, and A. Arias, "High impact velocity on multi-layered composite of polyether ether ketone and aluminium," *Composite Interfaces*, vol. 22, no. 8, pp. 705–715, Jun. 2015.

[19]   S. K. Sundaram, B. A. G, and A. B, "Influence of target dynamics and number of impacts on ballistic performance of 6061-T6 and 7075-T6 aluminum alloy targets," *Mechanics Based Design of Structures and Machines*, vol. 50, no. 3, pp. 993–1011, Mar. 2020.

[20]   N. Taniguchi, T. Nishiwaki, and H. Kawada, "Tensile strength of unidirectional CFRP laminate under high strain rate," *Advanced Composite Materials*, vol. 16, no. 2, pp. 167–180, Jan. 2007.

[21]   D. Gao *et al.*, "Effect of Strain Rate on Tensile Properties of Carbon Fiber-Reinforced Epoxy Laminates with Different Stacking Sequences and Ply Orientations," *Polymers*, vol. 15, no. 12, p. 2711, Jun. 2023.

[22]   J. Kwon, J. Choi, H. Huh, and J. Lee, "Evaluation of the effect of the strain rate on the tensile properties of carbon–epoxy composite laminates," *Journal of Composite Materials*, vol. 51, no. 22, pp. 3197–3210, Dec. 2016.

[23]   A. Fink and B. Kolesnikov, "Hybrid Titanium Composite Material Improving Composite Structure Coupling," *Spacecraft Structures, Materials and Mechanical Testing 2005*, vol. 581, May 2005.

[24]   J. Sun, A. Daliri, G. Lu, D. Liu, F. Xia, and A. Gong, "Tensile behaviour of titanium-based carbon-fibre/epoxy laminate," *Construction and Building Materials*, vol. 281, p. 122633, Feb. 2021.